New Astronomy 67 (2019) 97–102

Contents lists available at ScienceDirect

New Astronomy

journal homepage: www.elsevier.com/locate/newast

Photoionization of fine structure levels of Ne III

Sultana N. Nahar

Department of Astronomy, The Ohio State University, Columbus, OH 43210, USA

ARTICLE INFO

Keywords:
Ne III
Photoionization
Cross sections of excited levels
R-Matrix method
Resonant features 32.10-f
95.30.Ky
32.80-T

ABSTRACT

Detailed study on the characteristic features in photoionization of Ne III, ($h\nu$ + Ne III → Ne VI + e) is reported. The calculations were carried out in relativistic Briet–Pauli R-matrix (BPRM) method and close-coupling (CC) approximation. The CC expansion for the wavefunction of Ne III includes 58 fine structure levels of Ne IV from configurations $2s^22p^3$, $2s2p^4$, $2p^5$, $2s^22p^23s$, $2s^22p^23p$, $2s^22p^23d$. The photoionization cross section (σ_{PI}) features exhibit i) presence of prominent resonances in the low energy region near the ionization thresholds of low lying levels, ii) lower energy region of extensive narrow Rydberg resonances and slow decaying background cross section in the high energy region for equivalent electron levels, and iii) presence of strong Seaton resonances due to photo-excitation-of-core (PEC) in the high energy region. The relativistic effects have almost no impact on the σ_{PI} in the high energy regions. However, for a number of low lying levels the coupling of fine structure channels, which is not allowed in LS coupling, introduces high-peak narrow resonances with almost zero background below the excitation threshold of $2s^22p^3(^2D^o)$ level of the residual ion. These will enhance quantities such as electron-ion recombination, opacity at very low temperature. The Seaton resonances due to n = 3 PECs in the high energy region, which was not studied before, are more prominent than those for n = 2 PECs. For complete modeling of astrophysical and laboratory plasmas, photoionization cross sections are presented for a large number of excited levels, in total 392, with n ≤ 10 and $l \leq$ 9.

1. Introduction

Neon lines observed in astrophysical spectra, such as from planetary nebulae (e.g. Rubin et al., 2001; Rubin, 2004; Dance et al., 2013) and galaxies (e.g. Crockett et al., 2006), can be used for the diagnostics of the objects. The temperature and density diagnostics of nebular photoionized plasma can be determined by the observed Ne III lines. These lines are also common in the star-born galaxies (Ho and Keto, 2007) which produces more stars than typical 1–6 per year and the ionizing photons are produced by the young, hot, massive stars. The Ne lines can provide environmental diagnostics of metalicities, stellar populations, star formation rates and histories, and other interstellar medium properties (Dopita1 et al., 2006). The spectral analysis of the models require photoionization cross sections. Photoionization cross sections of Ne III have been recently measured at the Advanced Light Source (G. Hinojosa, private communication 2017) prompting high accuracy data needed for the benchmarking.

Very limited study has been carried out on the detailed photoionization of Ne III except for the R-matrix calculations by Butler and Zeippen under the Opacity Project (OP) (The Opacity Project Team, 1995, 1996). The data were not published, but are available at the OP database (TOPbase). Compared to the present work, the earlier work was carried out nonrelativistic LS coupling approximation and did not study the high energy features due to n = 3 excitations in the residual ion. The present results should provide more accurate and complete data for astrophysical and laboratory plasma modeling.

2. Theory

Photoionization is a well known process and described in literature (e.g. Pradhan and Nahar, 2011 book AAS). A brief outline is given below for the guidance of the readers. Photoionization occurs directly,

$$h\nu + X^+ \rightarrow e + X^{++}, \tag{1}$$

which provides only background cross sections. It can also occur through formation of an intermediate doubly excited autoionization state which leads either to autoionization (AI) where the electron goes to continuum or to dielectronic recombination (DR) where the electron is captured by emission of a photon.

$$e + X^{++} \leftrightharpoons (X^+)^{**} \leftrightharpoons \begin{cases} a)\ e{+}X^{++}(AI) \\ b)\ h\nu{+}X^{+}(DR) \end{cases} \tag{2}$$

The autoionizing state introduces a resonance in the process. The

E-mail address: nahar.1@osu.e+5du.
URL: http://www.astronomy.ohio-state.edu/~nahar.

https://doi.org/10.1016/j.newast.2018.09.011
Received 29 June 2018; Received in revised form 21 September 2018; Accepted 24 September 2018
Available online 25 September 2018
1384-1076/

autoionizing resonance can be described theoretically by including the excitations of the residual ion in the wave function, as considered in close coupling (CC) approximation here.

The CC approximation describes the atomic system of (N + 1) electrons by a 'target' or the 'core' or the residual ion of N-electrons interacting with the (N + 1)th electron. The total wave function, Ψ_E, of the (N + 1) electrons system in a symmetry $SLJ\pi$ is represented by an expansion as

$$\Psi_E(e + ion) = A \sum_i \chi_i(ion)\theta_i + \sum_j c_j \Phi_j, \tag{3}$$

where the target ion eigenfunction, χ_i, is coupled with the (N + 1)th electron function, θ_i. The first sum is over the ground and excited residual ion states. The (N + 1)th electron with kinetic energy k_i^2 is in a channel labeled as $S_i L_i J_i \pi_i k_i^2 \ell_i (SLJ\pi)$. In the second sum, the Φ_js are bound channel functions of the (N + 1)-electrons system that account for short range correlation and the orthogonality between the continuum and the bound electron orbitals.

The relativistic effects are included through Breit-Pauli approximation (e.g. Hummer et al., 1993; Pradhan and Nahar, 2011) where the Hamiltonian of the (N + 1)-electrons system in Rydberg unit (1/2 of Hartree) is written as

$$H_{N+1}^{\rm BP} = \sum_{i=1}^{N+1} \left\{ -\nabla_i^2 - \frac{2Z}{r_i} + \sum_{j>i}^{N+1} \frac{2}{r_{ij}} \right\} + H_{N+1}^{\rm mass} + H_{N+1}^{\rm Dar} + H_{N+1}^{\rm so} \tag{4}$$

The additional terms are the relativistic one-body correction terms, the mass correction, $H^{\rm mass} = -\frac{\alpha^2}{4}\sum_i {p_i}^4$, Darwin, $H^{\rm Dar} = \frac{Z\alpha^2}{4}\sum_i \nabla^2(\frac{1}{r_i})$, and the spin-orbit interaction, $H^{\rm so} = Z\alpha^2 \sum_i \frac{1}{r_i^3}\mathbf{l_i}.\,\mathbf{s_i}$. Under the Iron Project (IP, Hummer et al., 1993) the Bret-Pauli R-matrix (BPRM) method includes these and part of two-body interaction terms, which are without the momentum operators (e.g. Pradhan and Nahar, 2011).

Substitution of the CC wavefunction $\Psi_E(e + ion)$ in the Schrodinger equation

$$H_{N+1}\,\Psi_E = E\,\Psi_E \tag{5}$$

introduces a set of coupled equations that are solved using the R-matrix approach. The details of the R-matrix method in the CC approximation can be found in references (e.g. Burke and Robb, 1975; Seaton, 1987; Berrington et al., 1987; Berrington et al., 1995; Pradhan and Nahar, 2011). In BPRM method, the set of $SL\pi$ is recoupled for $J\pi$ levels of (e + ion) system which is followed by diagonalization of the Hamiltonian. The solution is a continuum wave function, Ψ_F, for an electron with positive energies (E > 0), or a bound state, Ψ_B, at a negative total energy (E ≤ 0).

Transition matrix elements for photoionization, $< \Psi_B||\mathbf{D}||\Psi_F >$ where $\mathbf{D} = \sum_i \mathbf{r}_i$ is the dipole operator and the sum is over the number of electrons, are obtained from the bound Ψ_B and continuum Ψ_F wave functions. The transition matrix element gives the generalized line strength **S** as

$$\mathbf{S} = |<\Psi_j||\mathbf{D}_L||\Psi_i>|^2 = \left| \left\langle \psi_f | \sum_{j=1}^{N+1} r_j | \psi_i \right\rangle \right|^2, \tag{6}$$

where Ψ_i and Ψ_f are the initial and final state wave functions and photoionization cross section (σ_{PI}) is obtained as,

$$\sigma_{PI} = \frac{4\pi^2}{3c}\frac{1}{g_i}\omega\mathbf{S}, \tag{7}$$

where g_i is the statistical weight factor of the bound state and ω is the incident photon energy. Radiation damping of the resonances (Zhang et al., 1999) has been included. The complex resonant structures in photoionization result from channel couplings between continuum channels that are open ($k_i^2 > 0$), and ones that are closed ($k_i^2 < 0$), at electron energies k_i^2 corresponding to autoionizing states of the Rydberg series, $S_i L_i J_i \pi_i \nu\ell$ where ν is the effective quantum number, converging to the target thresholds.

Table 1
Levels and energies (E_t) of the residual ion Ne IV included in the wavefunction expansion of Ne III, and comparison with observed values at the compiled table of the NIST.

	Level	J_t	E_t(Ry) NIST	E_t(Ry) SS
1	$1s^2 2s^2 2p^3(^4S^o)$	3/2	0.0	0.
2	$1s^2 2s^2 2p^3(^2D^o)$	5/2	0.375758	0.4143
3	$1s^2 2s^2 2p^3(^2D^o)$	3/2	0.37616	0.4139
4	$1s^2 2s^2 2p^3(^2P^o)$	3/2	0.5690	0.5796
5	$1s^2 2s^2 2p^3(^2P^o)$	1/2	0.5689	0.5793
6	$1s^2 2s 2p^4(^4P)$	5/2	1.6755	1.6906
7	$1s^2 2s 2p^4(^4P)$	3/2	1.6811	1.6961
8	$1s^2 2s 2p^4(^4P)$	1/2	1.6840	1.6993
9	$1s^2 2s 2p^4(^2D)$	5/2	2.3153	2.4326
10	$1s^2 2s 2p^4(^2D)$	3/2	2.3155	2.4325
11	$1s^2 2s 2p^4(^2S)$	1/2	2.7304	2.8349
12	$1s^2 2s 2p^4(^2P)$	3/2	2.9163	3.1095
13	$1s^2 2s 2p^4(^2P)$	1/2	2.9228	3.1162
14	$1s^2 2s^2 2p^2 3s(^4P)$	1/2	4.3622	4.3915
15	$1s^2 2s^2 2p^2 3s(^4P)$	3/2	4.3657	4.3949
16	$1s^2 2s^2 2p^2 3s(^4P)$	5/2	4.3710	4.4006
17	$1s^2 2p^5(^2P^o)$	3/2	4.4188	4.6890
18	$1s^2 2p^5(^2P^o)$	1/2	4.4275	4.6986
19	$1s^2 2s^2 2p^2 3s(^2P)$	1/2	4.4516	4.4976
20	$1s^2 2s^2 2p^2 3s(^2P)$	3/2	4.4579	4.5043
21	$1s^2 2s^2 2p^2 3p(^2S^o)$	1/2		4.7018
22	$1s^2 2s^2 2p^2 3s(^2D)$	5/2	4.6628	4.7094
23	$1s^2 2s^2 2p^2 3s(^2D)$	3/2	4.6630	4.7094
24	$1s^2 2s^2 2p^2 3p(^4D^o)$	1/2	4.7478	4.7572
25	$1s^2 2s^2 2p^2 3p(^4D^o)$	3/2	4.7498	4.7592
26	$1s^2 2s^2 2p^2 3p(^4D^o)$	5/2	4.7530	4.7626
27	$1s^2 2s^2 2p^2 3p(^4D^o)$	7/2	4.7573	4.7674
28	$1s^2 2s^2 2p^2 3p(^4P^o)$	1/2	4.7795	4.7965
29	$1s^2 2s^2 2p^2 3p(^4P^o)$	3/2	4.7812	4.7984
30	$1s^2 2s^2 2p^2 3p(^4P^o)$	5/2	4.7844	4.8018
31	$1s^2 2s^2 2p^2 3p(^2D^o)$	3/2	4.8367	4.8643
32	$1s^2 2s^2 2p^2 3p(^2D^o)$	5/2	4.8569	4.8710
33	$1s^2 2s^2 2p^2 3p(^4S^o)$	3/2	4.8569	4.8730
34	$1s^2 2s 2p^3 3s(^6S^o)$	5/2	4.9072	5.0673
35	$1s^2 2s^2 2p^2 3p(^2P^o)$	1/2		4.9367
36	$1s^2 2s^2 2p^2 3p(^2P^o)$	3/2		4.9372
37	$1s^2 2s^2 2p^2 3s(^2S)$	1/2	5.0301	5.1169
38	$1s^2 2s^2 2p^2 3p(^2F^o)$	5/2	5.0602	5.0983
39	$1s^2 2s^2 2p^2 3p(^2F^o)$	7/2	5.0614	5.0997
40	$1s^2 2s^2 2p^2 3p(^2D^o)$	5/2	5.1133	5.1863
41	$1s^2 2s^2 2p^2 3p(^2D^o)$	3/2	5.1143	5.1868
42	$1s^2 2s^2 2p^2 3p(^2P^o)$	1/2		5.2463
43	$1s^2 2s^2 2p^2 3p(^2P^o)$	3/2		5.2495
44	$1s^2 2s^2 2p^2 3d(^2P)$	3/2	5.2511	5.3040
45	$1s^2 2s^2 2p^2 3d(^4F)$	3/2		5.2679
46	$1s^2 2s^2 2p^2 3d(^4F)$	5/2		5.2697
47	$1s^2 2s^2 2p^2 3d(^4F)$	7/2		5.2725
48	$1s^2 2s^2 2p^2 3d(^4F)$	9/2		5.2761
49	$1s^2 2s^2 2p^2 3d(^2P)$	1/2	5.2547	5.3116
50	$1s^2 2s^2 2p^2 3d(^2D)$	3/2	5.2599	5.4149
51	$1s^2 2s^2 2p^2 3d(^2D)$	5/2	5.2599	5.4168
52	$1s^2 2s^2 2p^2 3d(^4P)$	5/2	5.2790	5.3275
53	$1s^2 2s^2 2p^2 3d(^4P)$	3/2	5.2819	5.3300
54	$1s^2 2s^2 2p^2 3d(^4P)$	1/2	5.2830	5.3313
55	$1s^2 2s^2 2p^2 3d(^4D)$	1/2		5.3059
56	$1s^2 2s^2 2p^2 3d(^4D)$	5/2		5.3090
57	$1s^2 2s^2 2p^2 3d(^4D)$	3/2		5.3092
58	$1s^2 2s^2 2p^2 3d(^4D)$	7/2		5.3109

3. Computation

The BPRM calculation involves number of stages of computations through the package of BPRM codes (Berrington et al., 1987; 1995). R-matrix computations begin at stage 1 using the code named STG1 which takes the wavefunction of the residual ion as the input. The wavefunction of the residual ion Ne IV has been obtained using the atomic

structure code SUPERSTRUCTURE (SS) (Eissner et al 1974, Nahar et al., 2003). SS uses Thomas-Fermi-Dirac-Amadi approximation with relativistic effects through Breit-Pauli approximation. A set of 17 configurations of Ne IV, $2s^22p^3$, $2s2p^4$, $2p^5$, $2s^22p^23s$, $2s^22p^23p$, $2s^22p^23d$, $2s^22p^24s$, $2s^22p^24p$, $2s^22p^24d$, $2s2p^33s$, $2s2p^33p$, $2s2p^33d$, $2s^22p3s^2$, $2s^22p3p^2$, $2s^22p3d^2$, $2s^22p4s^2$, $2s^22p4p^2$ where each configuration has filled $1s^2$ orbital, along with the set of Thomas-Fermi λ parameters for the orbitals as 1.47(1s), 1.27(2s), 1.19(2p), 1.22(3s), 1.32(3p), 1.1(3d), 1.15(4s), 1.1(4p). 1.0(4d) were used for the optimized wavefunctions. Table 1 presents the 58 fine structure levels going up to 3d orbital of Ne VI which were included in the Ne III wavefunction expansion. The level energies of Ne IV are compared with the observed values listed in the compiled table of NIST (http://www.nist.gov/pml/data/asd.cfm). Comparisons show good agreement between the observed (NIST compilation) and calculated energies. The accuracy of these energies improves that of (N + 1) electron ion. It may be noted that the R-matrix calculation can accommodate large number of configurations for the (N + 1)-electrons atomic system and thus raises the accuracy of the energies of ion. The positions of the resonances in photoionization are determined with respect to those of the residual ion. Hence the calculated energies of the residual ion are replaced by the observed energies, whenever possible, for more accurate resonance positions.

The angular momentum of the partial waves of the interacting electron is specified to be $0 \le \ell \le 11$. The R-matrix basis set of the orbitals inside the R-matrix sphere contains 14 terms and the R-matrix boundary was chosen to be large enough, 10 a_o, for the accommodate the short range potentials.

The second term of the wave function in Eq. (3), which represents the bound state correlation functions, included 95 configurations of Ne III with orbital occupancies from minimum to a maximum number as given within parentheses of the orbitals 1s(2-2), 2s(0–2), 2p (0–6), 3s(0–2), 3p (0–2), 3d(0–2), 4s(0–1), 4p(0–1). Computations are carried out for all angular momenta, $0 \le L \le$ 8–11 for septets, for quintets, triplets and singlets as needed for $0 \le J \le$ 8 levels of Ne III. The narrow resonances of photoionization were delineated at a fine energy mesh.

4. Results and discussions

Photoionization of Ne III (Ne III + $h\nu$ → Ne VI + e) is studied in detail for the characteristic features. These are reported for a large number of bound levels of Ne III, 392 fine structure levels in total, with $n \le 10$ and $l \le 9$. There are significant differences between the earlier and present R-matrix calculations for the ion. Compared to the earlier work, the present results are expected to be of higher accuracy and more complete due to i) relativistic fine structure effects not considered in LS coupling approximation, ii) implemented a larger wavefuntions which included excitations to levels of n = 2,3 complexes instead only within n = 2 complex of the residual ion, iii) obtained cross sections of more bound states with $l \le$ 9 instead of $l \le$ 3. Important characteristics in σ_{PI} are illustrated below.

The R-matrix calculation obtains the energies as the eigenvalues of the Hamiltonian matrix but without spectroscopic identification. The spectroscopic algorithm developed by Nahar (2000) is used to identify part of the energy set. The whole set of energies will be identified and published with radiative transitions in a separate paper. A comparison of calculated energies of Ne III with the measured values by Kramida and Nave (2006) available at the NIST compiled table is given in Table 2. The comparison shows the agreement between the two sets is less than 1% indicating higher accuracy of the data.

4.1. Relativistic fine structure effects

Fig. 1 presents σ_{PI} of the ground level of Ne III from (a) the present work and (b) the OP work by Butler and Zeippen (TOPbase). Resonances are found to form at and near threshold region of the photoionization cross section of the ground level $2s^22p^4(^3P_2)$ of Ne III. They

Table 2
Comparison of calculated levels energies of Ne III with the observed values at the compiled table of the NIST.

Level		J	E(Ry)	E(Ry)
			BPRM	NIST
$2s^22p^4$	^3P	2.0	4.714	4.662
$2s^22p^4$	^3P	1.0	4.709	4.656
$2s^22p^4$	^3P	0.0	4.706	4.653
$2s^22p^4$	^1D	2.0	4.465	4.426
$2s^22p^4$	^1S	0.0	4.151	4.153
$2s2p^5$	$^3P^o$	2.0	2.807	2.800
$2s2p^5$	$^3P^o$	1.0	2.803	2.795
$2s2p^5$	$^3P^o$	0.0	2.801	2.792
$2s2p^5$	$^1P^o$	1.0	2.007	2.024
$2s^22p^3(^4S^o)3s$	$^5S^o$	2.0	1.871	1.838
$2s^22p^3(^4S^o)3s$	$^3S^o$	1.0	1.773	1.751
$2s^22p^3(^4S^o)3p$	^5P	3.0	1.503	1.486
$2s^22p^3(^4S^o)3p$	^5P	2.0	1.504	1.486
$2s^22p^3(^4S^o)3p$	^5P	1.0	1.504	1.487
$2s^22p^3(^2D^o)3s$	$^3D^o$	3.0	1.434	1.444
$2s^22p^3(^2D^o)3s$	$^3D^o$	2.0	1.434	1.443
$2s^22p^3(^2D^o)3s$	$^3D^o$	1.0	1.434	1.443
$2s^22p^3(^4S^o)3p$	^3P	2.0	1.422	1.410
$2s^22p^3(^4S^o)3p$	^3P	1.0	1.423	1.411
$2s^22p^3(^4S^o)3p$	^3P	0.0	1.423	1.410
$2s^22p^3(^2D^o)3s$	$^1D^o$	2.0	1.393	1.400
$2s^22p^3(^2P^o)3s$	$^3P^o$	2.0	1.253	1.249
$2s^22p^3(^2P^o)3s$	$^3P^o$	1.0	1.253	1.249
$2s^22p^3(^2P^o)3s$	$^3P^o$	0.0	1.253	1.249

belong to the autoionizing series of levels, $^2D^o_{3/2,5/2}\nu l$ and $^2P^o_{1/2,3/2}\nu l$ that converge to the residual ion excitation levels $^2D^o_{3/2,5/2}$ and $^2P^o_{1/2,3/2}$. ν is the effective quantum number. These converging thresholds have average energies approximately at 5.05 Ry for $^2D^o$ and 5.25 Ry for $^2P^o$ as indicated by arrows in Fig. 1. The comparison shows very similar structures and background cross sections in both panels except additional resonances in (a) belonging to residual ion excitations to the n = 3 levels not considered under the OP (b). These additional resonances are weak. No significant contribution from the BPRM relativistic effects from the present work can be noticed. Relativistic effects are not usually expected to be significant for the low Z neon.

However, as found earlier (e.g. Nahar, 2002 for C II) relativistic effects are seen as important contributor at very low energy region for lower Z elements. These contributions come in the form of resonant structures formed by the couplings of fine structure channels which are not allowed in LS coupling approximation. Typically these resonances are narrow and high-peak, but have almost zero background cross sections. For the low lying Ne III $2s^22p^4(^1D_2)$ level these resonances, as seen in Fig. 2, form below the excited $^2D^o$ state of residual ion Ne IV but can not form in LS coupling. The difference in features is illustrated in Fig. 2. ^1D photoionizes to states $^1P^o$ $^1D^o$, $^1F^o$. In LS coupling these states can not form below $^2D^o$ since they do not couple to the residual ion ground level $^4S^o$ state but couple to $^2D^o$ state of the residual ion. Fig. 2 shows these resonances in panel (a) obtained in the present work filling almost the entire energy region between $^4S^o$ and $^2D^o$ states. The present σ_{PI} is compared with that in LS coupling obtained under the OP in panel (b) where the cross sections start at $^2D^o$ state. The OP σ_{PI} is shifted some to the left as its ionization energy is lower than the present value. Nonetheless the features are similar in both plots. In BPRM approximation, the continuum fine structure channels $^4S^o_{3/2}\varepsilon d(^3D^o_{1,2,3},^5 D^o_{1,2,3})$ and $^4S^o_{3/2}\varepsilon s(^3S_1,^5 S^o_2)$ can couple to $^1P^o_1,^1 D^o_2,^1 F^o_3$ and hence form the resonances from $^4S^o$. These resonances have been observed in the experimental spectrum of the photoionizaton (G. Hinojosa, private communication 2017). These low energy resonances is found to appear only for limited number of levels of Ne III. In the high energy region fine structure effects are found to be negligible. Hence the relativistic effects will increase the overall accuracy of the cross sections but may have limited contributions for quantities, such as total recombination rates.

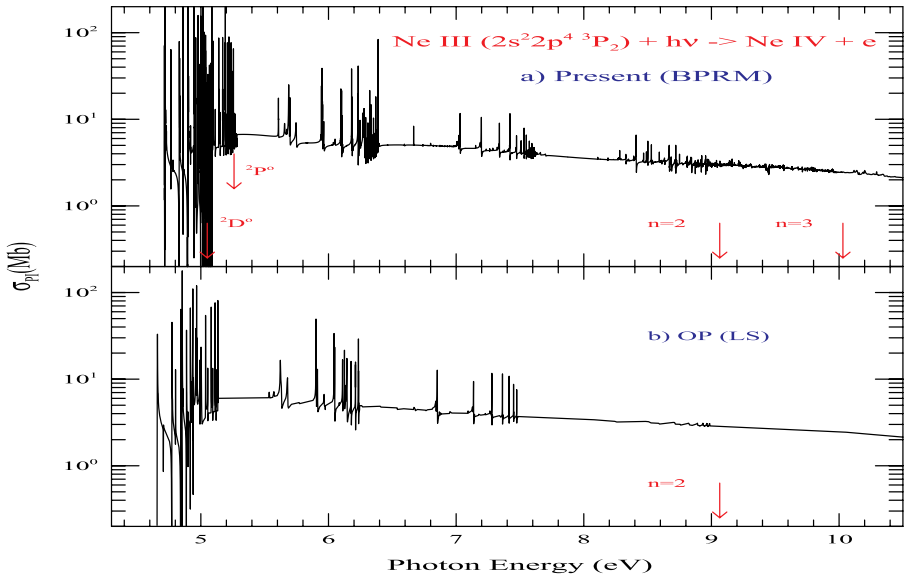

Fig. 1. Photoionization cross sections σ_{PI} of the ground level $1s^2\,2s^2\,2p^4(^3P_2)$ of Ne III: from a) the present BPRM calculations, b) by Butler and Zeippen (TOPbase). The cross sections look similar except for the additional resonances in the high energy region in (a) due to n = 3 excitations in the core ion.

4.2. Photoionization of equivalent electron levles

The equivalent electron levels show characteristics features that play significant role in low to high temperature plasma applications. The equivalent electron levels, which exists in limited number for an atomic system, typically lie in the low energy region. However, they are important contributors in applications due to extensive resonant features in the lower energy region and slow decaying background cross section in the higher energy region. Fig. 3 presents σ_{PI} of two equivalent electron levels, (a) $2s2p^5(^1P_1^o)$ and (b) $2s2p^5(^3P_2^o)$ demonstrating the features. Panel (a) shows resonances converging on to various excited thresholds (states are averaged over fine structure components and pointed by arrows) of the residual ion and enhancement of the background cross section at the thresholds. Beyond the highest excited threshold of the residual ion, the enhanced background continues to remain strong and hence the integration over a large energy range will make a significant contribution. Panel (b) shows similar features with slow decaying background cross section for the level $2s2p^5(^3P_2^o)$.

4.3. Seaton resonances in photoionization of excited states

One common feature in photoionization of excited states with a single valence electron is the presence of Seaton resonances due to photoexcitation-of-core (PEC) (Yu and Seaton, 1987). A Seaton resonance is introduced when the core ion absorbs the photon for a dipole allowed transition from its ground state before leading to ionization. These resonances can be wide with enhanced background and are typically embedded in narrow Rydberg resonances. Since the resonances correspond to transition energies of the core ion their energy positions remain the same regardless of the ionization energies of the photoionizing levels. Fig. 4 presents σ_{PI} of four excited levels illustrating features of Seaton resonances. The levels are arranged in order of their high to low ionization potential, (a) $2s^2 2p^3(^4S^o)3p(^3P_1)$, (b) $2s^2 2p^3(^2P^o)3p(^3S_1)$, (c) $2s^2 2p^3(^4S^o)4s(^3P_2^o)$, (d) $2s^2 2p^3(^2D^o)4p(^3D_1)$ (also obvious from the position of the threshold cross sections). The energy positions of Seaton resonances are indicated by the arrows in each panel. They correspond to the dipole allowed transitions ($\Delta J = 0, \pm 1$ and change of

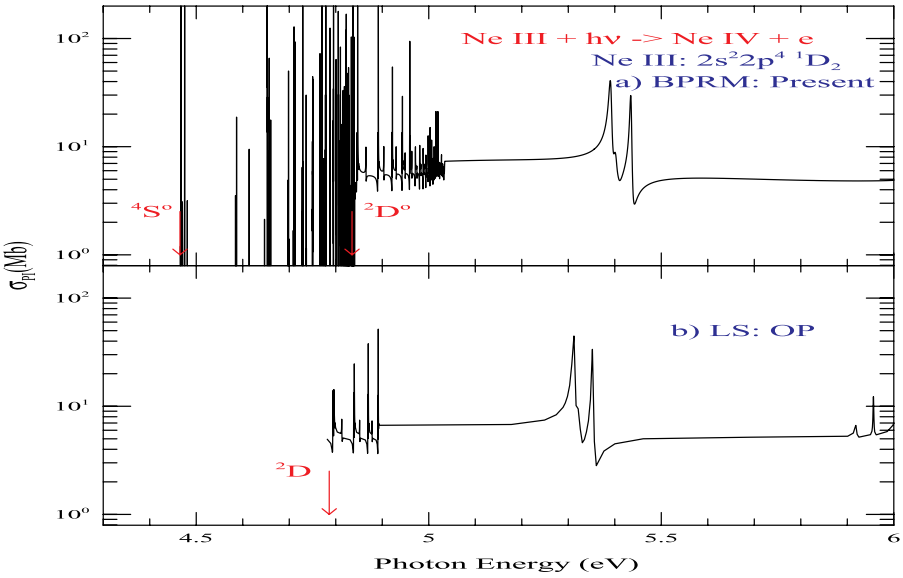

Fig. 2. Photoionization cross sections σ_{PI} of the $1s^2\,2s^2\,2p^4(^1D_2)$ level of Ne III: from a) the present BPRM calculation, b) Butler and Zeippen (TOPbase). The cross sections look similar except for the additional resonances below the $^2D^o$ threshold of the residual ion in (a) arising from couplings of fine structure channels that are not allowed in LS coupling.

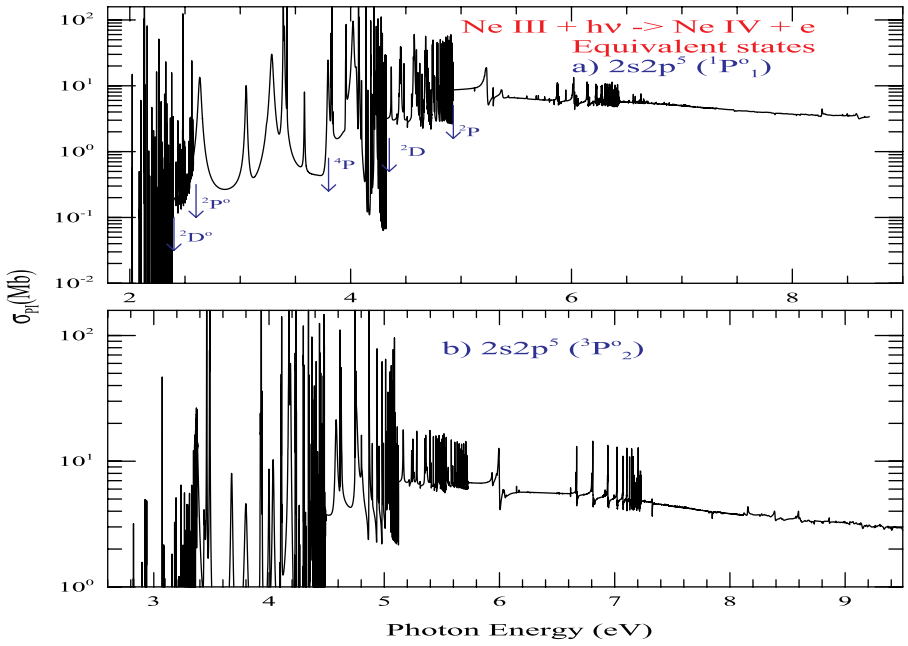

Fig. 3. Photoionization cross sections σ_{PI} of the excited equivalent electron levels (a) $2s2p^5(^1P^o_1)$ and (b) $2s2p^5(^3P^o_2)$ demonstrating the strength of the levels with resonant features in the lower energy region, enhancement at the excited thresholds of the residual ion (arrows in panel a) and slow decaying background cross sections.

parity) from $^4S^o_{3/2}$ to levels listed in Table 1. It can be noted that Seaton resonances become more prominent with higher excited levels of Ne III. The prominence of the resonances is maximum in the high energy region, particularly for the level $2s^22p^3(^2D^o)4p(^3D_1)$ (panel d) where the background cross section is enhanced by few orders of magnitude. The high energy Seaton resonances form due to PECs to n = 3 levels in the energy region of 4.3 - 5.3 Ry (Table 1) of the core ion not considered under the OP. These resonances will contribute more in applications in the high temperature region.

5. Conclusion

Characteristic features in photoionization cross sections of Ne III have studied in detailed using relativistic BPRM method for 392 bound levels with n $\leq$ 10 and $l \leq 9$. Study considers a wavefunction expansion of 58 levels of the residual ion with excitations up to 3d orbitals that show dominant features not observed in earlier calculations with excitations up to 2p. Resonances are delineated and relativistic effects are important in the low energy regions of a number of levels. Seaton

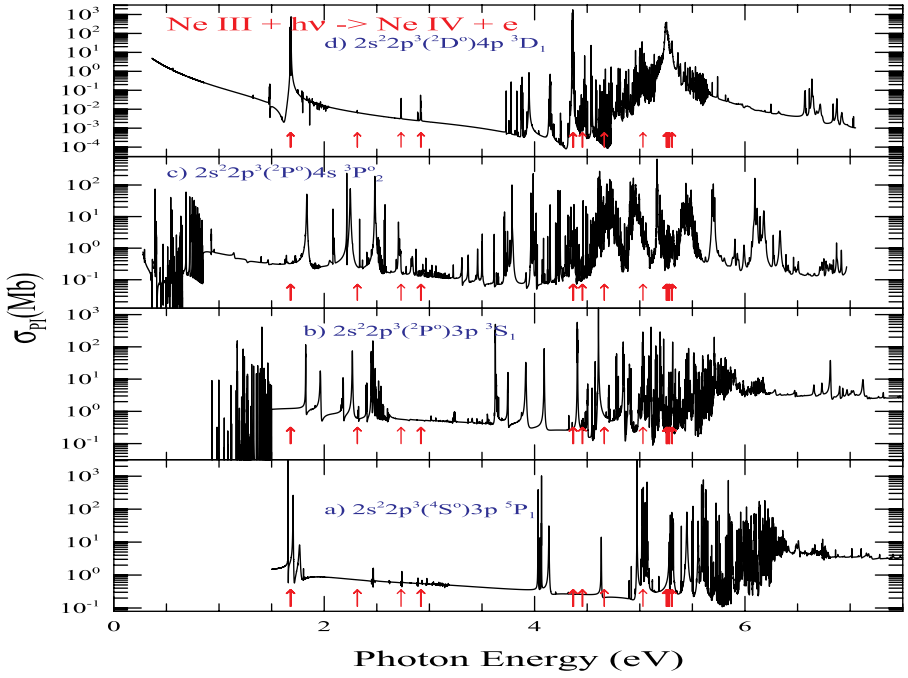

Fig. 4. Photoionization cross sections σ_{PI} of excited levels, (a) $2s^22p^3(^4S^o)3p(^3P_1)$, (b) $2s^22p^3(^2P^o)3p(^3S_1)$, (c) $2s^22p^3(^4S^o)4s(^3P^o_2)$, (d) $2s^22p^3(^2D^o)4p(^3D_1)$ of Ne III. Prominent Seaton resonances due to core ion excitation to various electric dipole allowed levels are indicated by the arrows. These resonances enhance the background σ_{PI}, particularly those due to n = 3 transitions between 4.3 - 5.3 Ry for higher excited levels in panels (c) and (d).

resonances dominant the high energy region of excited levels. Work in progress for comparison of cross sections with the measured photoionization spectrum at ALS at Berkeley. The present cross sections are expected to be of high accuracy of about 10–15% based on (i) inclusion of relativistic effects, (ii) higher resolution for resonances, (iii) consideration of large number configurations, and (iv) accuracy in the ionization energies.

All photoionization data are available electronically from NORAD-Atomic-Data (NaharOSURadiativeAtomicData) website: www.norad.astronomy.ohio-state.edu/

Acknowledgments

This work was supported partially by the grants of National Science Foundation AST-1312441 and U.S. Department of EnergyDE-SC0012331. The computational work was carried out at the Ohio Supercomputer Center in Columbus Ohio.

References

Berrington, K.A., Burke, P.G., Butler, K., Seaton, M.J., Storey, P.J., Taylor, K.T., Yu, Y., 1987. Computational Methods. J. Phys. B 20, 6379–6397.
Berrington, K.A., Eissner, W., Norrington, P.H., 1995. Comput. Phys. Commun. 92, 290–420.
Burke, P.G., Robb, W.D., 1975. Adv. At. Mol. Phys. 11, 143–214.
Butler, K., Zeippen, C. J.,. Unpublished, Data available at the OP database TOPbase.
Crockett, N.R., Garnett, D.R., Massey, P., Jacoby, G., 2006. ApJ 637, 741–751.
Dance, D., Palay, E., Nahar, S. N., Pradhan, A. K., 2013. MNRAS 435, 1576–1581.
TOPbase. The Opacity Project database: http://cdsweb.u-strasbg.fr/topbase/topbase.html.
Dopita1, M.A., Fischera, J., Sutherland, R.S., Kewley, L.J., Tuffs, R.J., Popescu, C.C., van Breugel, W., Groves, B.A., Leitherer6, C., 2006. ApJ 647, 244–255.
Ho, L.C., Keto, E., 2007. ApJ 658, 314–318.
Hummer, D.G., Berrington, K.A., Eissner, W., K., P.A., Saraph, H.E., Tully, J.A., 1993. Astron. Astrophys. 279, 298–309.
Kramida, A.E., Nave, G., 2006. Eur. Phys. J. D 37, 1–21.
Nahar, S.N., 2000. Astron. Astrophys. Suppl. Ser. 147 (253).
Nahar, S.N., 2002. Phys Rev A 65, 052702.
Nahar, S.N., Eissner, W., Chen, G.X., Pradhan, A.K., 2003. A&A 408, 789.
NIST,. http://www.nist.gov/pml/data/asd.cfm.
Pradhan, A.K., Nahar, S.N., 2011. Atomic astrophysics and spectroscopy (AAS). Cambridge University Press.
Rubin, R.H., 2004. Proc. IAU Symp. 217. In: Duc, P.A., Braine, J., Brinks, E. (Eds.), Recycling Intergalactic and Interstellar Matter. Astron. Soc. Pac. pp. 190. San Francisco
Rubin, R.H., Dufour, R.J., Geballe, T.R., Colgan, S.W.J., Harrington, J.P., Lord, S.D., Liao, A.L., Levine, D.A., 2001. ASP Conf. Ser. In: Ferland, G., Savin, W.D. (Eds.), Spectroscopic Challenges of Photoionized Plasmas. Astron. Soc. Pac. Vol. 247. pp. 47. San Francisco
Seaton, M.J., 1987. J. Phys. B 20, 6363–6378.
The Opacity Project Team, 1995. The Opacity Project. Vol. 1 Institute of Physics Publishing. Vol. 2 (1996)
Yu, Y., Seaton, M.J., 1987. J. Phys. B 20, 6409–6429.
Zhang, H.L., Nahar, S.N., Pradhan, A.K., 1999. J. Phys. B 32, 1459.